Reduced graphene Oxide/NiO based nano-composites for the efficient removal of alizarin dye, indigo dye and reduction of nitro aromatic compounds

Renu Verma [a], Manmohan Singh Chauhan [a,*], Saurabh Pandey [a], Anshu Dandia [b]

[a] ASAS, Amity University Rajasthan, Jaipur, 303002, India
[b] Department of Chemistry, University of Rajasthan, Jaipur, 302004, India

ARTICLE INFO

ABSTRACT

Removal of alizarin red S (ARS) and Indigo dye from aqueous media and reduction of nitro aromatic compounds are successfully done under mild condition by using reduced Graphene Oxide-Nickel Oxide (rGO-NiO) nanocomposite as catalyst. RGO-NiO is well characterized by different analytical techniques. Morphology, structural, and composition studies done by HRTEM, FESEM, EDX, TGA, FTIR, XPS, Raman spectroscopy, and XRD. RGO-NiO nanocomposite has high stability for the removal of ARS, Indigo dye, reduction reaction nitro aromatic compounds.

1. Introduction

Industrialization has changed human life, but it has also caused significant changes in the environment. Environmental pollution is a serious problem these days, due to the increasing textile and paint industries. In these industries, several synthetic dyes and nitro aromatic compounds are utilized, which are extremely poisonous and dangerous to life due to their non-biodegradability [1]. These chemicals affect the environment in a variety of ways, particularly through waste water, because a large volume of water is utilized in the paint and textile industries and becomes contaminated [2]. As a result, it is critical to cleanse wastewater before discharging it into the environment [3]. To breakdown these chemicals, conventional wastewater treatment processes are applied. These typical wastewater treatment plants remove a very tiny amount of these chemicals, and the majority of these contaminants enter the reviving water. Alizarin Red S (ARS) dye is an anionic dye and carcinogenic materials [4]. Because of its complex structure of aromatic rings, it has high resistance to biodegradation and destruction under normal conditions. Indigo Carmine dye is the oldest dye commonly used in textile industries and also used in food dye, mainly in juice factories [5]. Inhaling, ingesting, or absorbing ARS and indigo dye can cause severe injury or irritation to the lungs, mucous membranes, eyes, skin, and respiratory tract. Because this dye is a stubborn and long-lasting contaminant, scientists have worked hard to design and construct an effective, easy, and cost-effective decontamination technique [6,7]. There are various methods to remove nitro-aromatic compounds and dyes from wastewater such as photo catalysis, biological degradation, removal and catalytically reductions [8,9]. Different semiconductor metal oxides, such as TiO_2, WO_3, ZnO, and CdS, have been used as photocatalyst for organic pollutant degradation and hydrogen production by photolysis of water [5,10]. Many literatures have reported the catalytical reduction of nitro-aniline by using TiO_2 as photo catalyst [11,12], transition metals (Cu, Ni), and Nobel metals (Pt, Pd, Au) [13]. However, all these methods have some limitations of reaction conditions such as high temperature,

---

* Corresponding author.
E-mail address: mschauhan@jpr.amity.edu (M.S. Chauhan).

high reaction time, high cost, reaction procedure and environmentally friendly. To overcome these problems eco-friendly and cheap catalyst was prepared via graphene oxide used as support material for metals. To boost removal and dye degradation efficiency, graphene-based nanomaterials were combined with co-catalysts, noble metal particles, metallic, non-metallic doping, and hydrogels [14]. Despite the fact that many researchers have reported on dye degradation by using graphene-based nickel nanocomposite (RGO-Ni) demonstrated better removal efficiency than other adsorbents such as TiO_2 and graphene TiO_2 [15], CuS/PVA nano-composite [16], and other self-assembled GO nanostructures from various styles [17].

Graphene as a material has so much potential and interest in research area due to its wide range of applications, its low cost, easy to use and scalability. Graphene can be easily converted into graphene oxide by oxidation reaction, it contains large number of oxygen functional group that is make graphene oxide (GO) more useful [18]. The hexagonal structure of GOs protects functional groups such as hydroxyl, epoxide, carboxyl, and some randomly dispersed alkyl groups in the plane. In the basal planes, hydroxyl and epoxide functional groups are close together, whereas carboxyl and alkyl groups are near the edges of GO flakes. Longer oxidation durations convert more hydroxyl groups to epoxide groups in the basal plane. Graphene oxide (GO) has been produced using the methods of Brodie, Staundenmaier, Offeman, and Hummers since the early nineteenth century. These methods rely on oxidizing graphite with powerful acids and oxidants. The qualities of GO are critical for getting the desired attributes of rGO [19].

Herein, we have reported the successful reduction of 4-nitroaniline, picric acid, and removal of ARS and Indigo dye in aqueous medium by using reduced graphene oxide based on nickel oxide nanocomposite. Catalyst shows good adsorbent property, because graphene has large surface area and high removal capacity. In addition, the reaction process is eco-friendly. Prepared catalyst was characterized by XRD, FESEM-EDX, HRTEM, TGA, and FTIR. Removal of dye and reduction of nitro aromatic compounds are examined by using UV spectroscopy.

2. Experimental procedure

2.1. Materials

All chemicals are purchased from Merck Chemicals and used without any further purification. Graphite powder, Alizarin Red S (ARS), Indigo dye, 4-Nitro-aniline (4-NA), picric acid, sulphuric acid (H_2SO_4), sodium nitrate ($NaNO_3$), hydrogen peroxide (H_2O_2), potassium permanganate ($KMnO_4$), nickel chloride hexa hydrate ($NiCl_2 \cdot 6H_2O$), and distilled water are used.

2.2. Preparation of graphene oxide

Graphene oxide is obtained from graphite powder by using modified Hummer's method [20]. Graphite powder is slowly added in the solution of concentrated sulphuric acid, sodium nitrate, and potassium permanganate. This reaction mixture is stirred in ice bath. After 2 h reaction mixture will become pasty and black-greenish. Furthermore, reaction mixture is placed at 35 °C in an oil bath for 30 min. Next, slowly addition of distilled water (200 ml) and the solution allowed to heat up to 90 °C for 3 h until color change into a little yellowish. H_2O_2 is added carefully (5%, 100 ml) to remove the excess of $KMnO_4$. Resultant solution filtered to collect the cake and wash it with distilled water for several times. After that, sonicate it for 1 h in distilled water, centrifuge the mixture 3 times (5000 rpm for 15 min).

2.3. Preparation of RGO-NiO nanocomposite

The rGO-NiO nanocomposite is prepared using the below method [21]. In this method, 5 ml of GO (1 mg ml^{-1}) in distil water is added in conical flask and sonicate the mixture at room temperature for 20 min. 38 mg of $NiCl_2 \cdot 6H_2O$ is added in it and again allow to sonicated for 30 min. After that, aqueous solution of sodium borohydride (5 ml of 0.1 M) is added into the solution. Precipitates are washed with distilled water and centrifuge the solution for three times (4000–6000 rpm). The washed precipitates are dried in an oven for 3 h and stored for further use. RGO-NiO is characterized by XRD, TGA, HR-TEM, FE-SEM, FTIR, XPS, Raman spectroscopy, and EDX.

2.4. Material characterization

RGO-NiO is characterized by different analytic techniques. FTIR spectral analysis is performed with Thermo scientific. The XRD pattern of the prepared catalyst is done with Rigaku SmartLab 9 kW rotating anode x-ray diffractometer. TGA curve of the sample is analyzed with NETZSCH STA 449F1 up to temperature range is 25 °C–800 °C. Microstructural and morphology studies of the catalyst is performed by FESEM with EDX (Carl Zeiss Ultra Plus) and HRTEM (FP 5022/22-Tecnai G2 20 STWIN). The X-ray Photoelectron Spectroscopy (XPS) of pallet form of the sample is done with Omicron ESCA (Electron Spectroscope for Chemical Analysis)From: Oxford Instrument Germany, Hemispherical Analyzer is used with mean radius is 124 mm, inner radius is 120.8 mm, and outer radius is 127.2 mm. Al anode is used for samples and its energy is 1486.7 eV. Angle between Analyzer and Source is 85°. Monochromatic X-ray is used and its resolution is confirmed by FWHM about 0.60 eV. Raman spectral with PL analysis is performed over STR500 Airix with laser 532 nm. Removal and reduction reaction are examined by UV-spectroscopy with wavelength range 200 nm–800 nm.

2.5. Optimization for catalytic performance

RGO-NiO nanocomposite is prepared for reduction of 4-NA, picric acid, and removal of ARS dye and indigo dye in aqueous medium.

To check the best performance of the catalysts for reduction reaction, the effect of catalyst loading on the reduction of nitro-aniline is observed. Different catalyst loading 1 mg, 2 mg, 3 mg, 4 mg, and 5 mg are performed at fixed reaction conditions. The effect of amount of sodium borohydride on reduction is also observed. From Table 1, it is clear that when 4 mg catalyst and 1 mmol of sodium borohydride are used, provides best results (Entry 4, Table 1).

2.6. Catalytic performance

2.6.1. Reduction of 4-nitro-aniline and picric acid

The catalytic activity of rGO-NiO is studied in reduction of 4-NA and picric acid. In experiment, 1 ml of $NaBH_4$ (37 mg in 1 ml) is added into aqueous solution of 4-Nitro-aniline (14 mg in 15 ml), and 4 mg of catalyst is added to the reaction mixture and stirrer it at room temperature. After complete the reduction, the yellow color of the solution became colorless. 4-NA is successfully reduced into 4 phenyldiamine. Same procedure is followed for the reduction of picric acid. In brief, I ml of sodium borohydride is added into aqueous solution of Picric acid (14 mg in 15 ml) and 4 mg of catalyst added into reaction mixture and stirrer it at room temperature. Picric acid successfully reduced into picramic acid. The reduction of the 4-NA and picric acid is examined by using UV spectroscopy. Scheme 1, shows the possible catalytical reduction mechanism of 4NA by using $NaBH_4$ and rGO-NiO nanocomposite. The addition of hydrogen molecules from the borohydride ion produced amino phenol with the release of water as by product.

A possible mechanism for the reduction of nitroaniline is presented in Scheme 1. Initially, nitro group got reduced to *N*-hydroxylamine oxide through hydride addition at oxygen of nitro group. Then, *N*-hydroxylamine oxide got reduced to dihydroxyl amine further it condensed into nitroso group by the removal of water [22]. Nitroso group got reduced to amino product by direct addition of hydrogen across the double bond. Finally, amino products were desorbed from the surface of rGO-NiO into solution which was confirmed from the UV–visible spectrum. Therefore, adsorption of reactant molecules, reduction of nitro to amino group followed by desorption of products from the surface catalyst were possible steps involved in the present reduction reaction. Scheme 2 represent the catalytical reduction for picric acid.

2.6.2. Removal of alizarin red S dye (ARS)

Removal of ARS dye is performed by using rGO-Ni catalyst. In experiment, 37 mg of sodium borohydride and 5 mg of rGO-NiO is added into 15 ml with 100 ppm of ARS, stirrer reaction mixture at room temperature until the color of solution change into pale yellow solution (Scheme 3). The supernatant ARS dye concentration is determined via UV–Visible spectrophotometer.

2.6.3. Removal of indigo dye

Prepared catalyst is also used for removal of indigo dye from aqueous medium. In experiment, 37 mg of sodium borohydride and 5 mg of rGO-NiO is added into 15 ml with 100 ppm of indigo dye, stirrer reaction mixture at room temperature until the dark blue color of solution change into colorless solution (Scheme 3). The supernatant dye concentration is determined via UV–Visible spectrophotometer. The percentage of dye removal is calculated using Eq. (1).

$$\% \, Removal = \frac{(Ao - A) * 100}{Ao} \tag{1}$$

Where, A_0 is the initial absorbance of the dye solution before treatment and A is the dye absorbance after removal.

2.7. Dye degradation kinetics

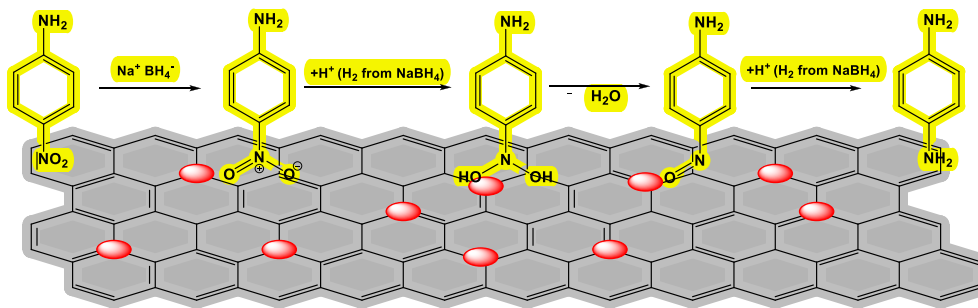The experimental findings fit the Langmuir-Hinshelwood (L-H) kinetic model. (Eq. (2)):

$$\frac{1}{R} = \frac{1}{Kr} + 1 \Big/ KrKC \tag{Eq (2)}$$

where r (mg/(L min) is the breakdown rate of the reactant, C (mg/L) is the reactant concentration, K is the equilibrium constant for dye adsorption on Kinnow peel powder (Langmuir constant), and kr (mg/(L min)) is the specific reaction rate constant for reactant
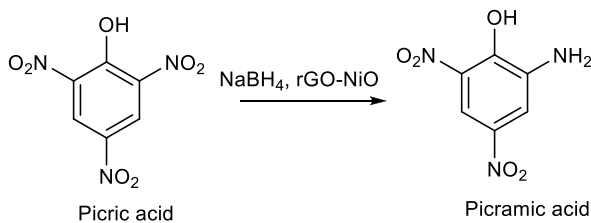
Table 1
Optimization table for reduction of 4-Nitro aniline via rGO-NiO nanocomposite. (a) Reaction condition for ARS dye and (b) reaction condition for Indigo dye.
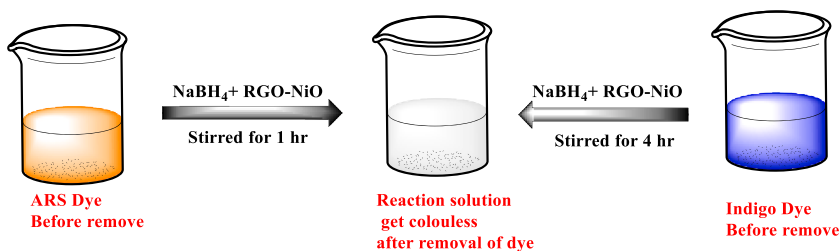
Entry	Catalyst loading (mg)	Sodium borohydride loading (mmol)	Reduction time (h)
1	1	1	Not complete reduction
2	2	1	Not complete reduction
3	3	1	4
4	4	1	2
5	4	0.6	3.50
6	4	0.75	3.30
7	5	1	2
8[a]	4	1	1
9[b]	4	1	4

Scheme 1. Possible Catalytical reduction mechanism of 4-NA.

Picric acid

Picramic acid

Scheme 2. Catalytical reduction reaction of Picric acid.

**ARS Dye
Before remove**

**Reaction solution
get colouless
after removal of dye**

**Indigo Dye
Before remove**

Scheme 3. Schematic representation of removal of ARS dye and indigo dye from aqueous medium by using prepared catalyst.

oxidation. However, adsorption/desorption equilibrium must be created under irradiation and in catalysis successes, which is a crucial problem needed for the L-H model's validity. The integral version of Eq. (3) is an obvious first order equation when the chemical concentration C is milli molar solution:
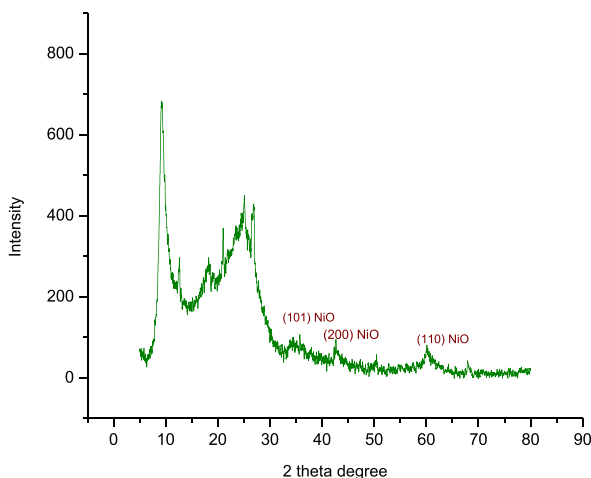
Fig. 1. XRD pattern of reduced GO-NiO nanocomposite.

$$In \frac{Ct}{Co} = KrKt = Kapp \ t \qquad \text{Eq (3)}$$

k_{app} is the apparent first order rate constant of photocatalytic degradation, and t is the reaction time. A straight line with the slope equal to the apparent first order rate constant k_{app} is shown by a plot of ln (Ct/Co) versus time. First order kinetics is generally applicable for various experiments that were pretty well suited by this kinetic model.

3. Result and discussion

In this article, reduced graphene oxide-based nickel oxide nanocomposite catalyst is synthesized. Firstly, modified Hummer's method is used for preparation of GO and after that nickel oxide was composed on graphene oxide. Morphology, structural, and thermal properties of rGO-NiO are characterized by using FTIR spectroscopy, HRTEM, FESEM with EDX, XRD, XPS, Raman spectroscopy and TGA. The supernatant ARS dye and indigo dye concentration and reduction of nitro aromatic compounds are determined via UV–Visible spectrophotometer.

Fig. 1 depicts the XRD patterns of the prepared catalyst. XRD graph clearly shows the catalyst is made up of crystalline NiO phases. NiO shows crystalline structure with diffraction peaks at 37.3, 43.3, and 62.9 are respectively indexed to the (101), (200), and (110) [21] which matches well with JCPDS card no. 00-044-1159. There is a diffraction peak near 24°, this is belonging to reduced graphene oxide [23]. The sharp peak at near 10°, this is belonged to the graphene oxide [24].

The comparative Fourier Transform Infrared pattern of graphene oxide and rGO-NiO nanocomposite are shown in Fig. 2. The main peaks detected at 3349, 1632, 1463, 1239, and 870 cm^{-1} in the given pattern are recognized to the O–H, C=C, *C*–OH, *C*–C, and C–O, respectively. Because of the partially reduction of oxygenated functional groups during the reaction, the intensities of these peaks reduced dramatically following the formation of NiO nanoparticles on rGO sheets. Indeed, after reducing GO with sodium borohydride, the peaks caused by *O*–H, *C*–O, and *C*–O stretching reduced considerably, with some disappearing totally.

TGA analysis is used to study the thermal characteristics of the prepared nanocomposite (Fig. 3). The first mass loss (22.39%) observed at below 167 °C is caused by the elimination of moisture content and water content. The degradation of the rGO's labile oxygenated functional groups is responsible for the second mass loss (18.96%) in the temperature range of 167–389 °C. Third mass loss (40.81%) observed above 500 °C results from the pyrolysis of the carbon skeleton of reduced graphene oxide nanosheet.

The surface study of the rGO-NiO is done by using SEM and HRTEM. SEM images clearly shows the presence of flakes of graphene in the prepared catalyst. The nickel oxide particles are distributed randomly throughout the graphene sheet (Fig. 4 (A, B)). On the curled morphology of the reduced graphene oxide, NiO particles are dispersed. SEM pictures show the NiO particles have nanosheet-based irregular structures. Moreover, the morphology of prepared rGO-NiO is done by HRTEM. HRTEM pictures of rGO-NiO show the shape of NiO particles as well (black spots) (Fig. 5 (A)) and the average size of the NiO composites (9 nm). Selected area electron diffraction (SAED) pattern given in Fig. 5(B) shows the lattice fringe can be easily noticed and interplanar gap is 0.25 nm, corresponding to the interplanar (110) and (101) NiO plane, thus confirms the presence of high crystallinity rGO-NiO nanocomposite [25].

Table 2 depicts the element present in rGO-NiO nanocomposite catalyst by using EDX. Because O and Ni elements are present, the particles composed to GO sheets are made of NiO. Inset Table 2 showing the elemental analysis, the atomic % ratio of O and Ni are 73.25%, 26.75%, and weight % are 26.75 and 57.27 respectively. All of these observations point to the effective synthesis of rGO-NiO catalyst.

Fig. 6 depicts the Raman spectra of GO and rGO-NiO. The Raman spectra of GO exhibits two notable peaks at 1352.4 cm^{-1} (D band) and 1605.3 cm^{-1} (G band). The peak intensity ratio of the D and G bands (ID/IG) is widely employed as a measure of the degree of
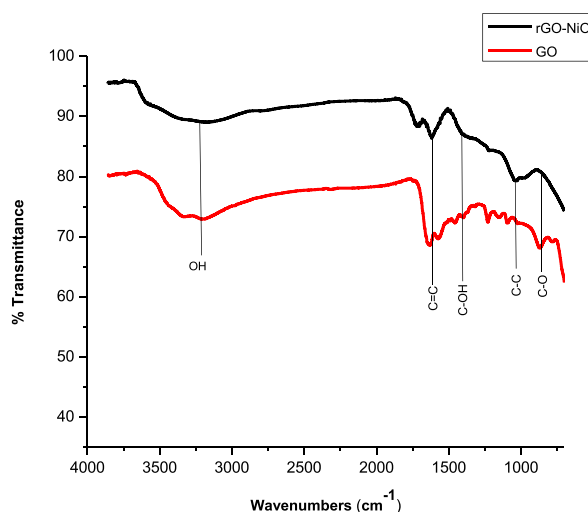

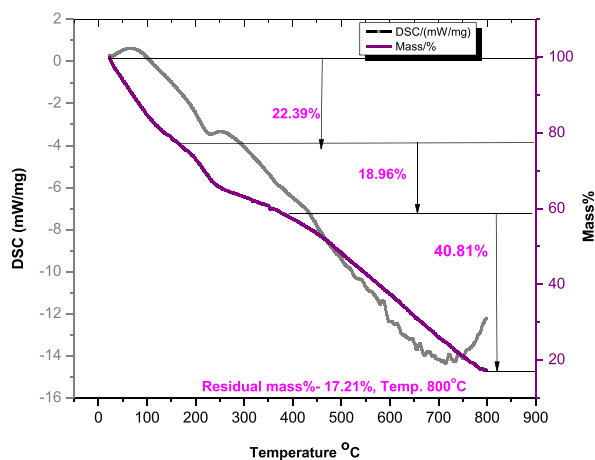**Fig. 2.** Comparative FTIR graph of GO and rGO-NiO nanocomposite.

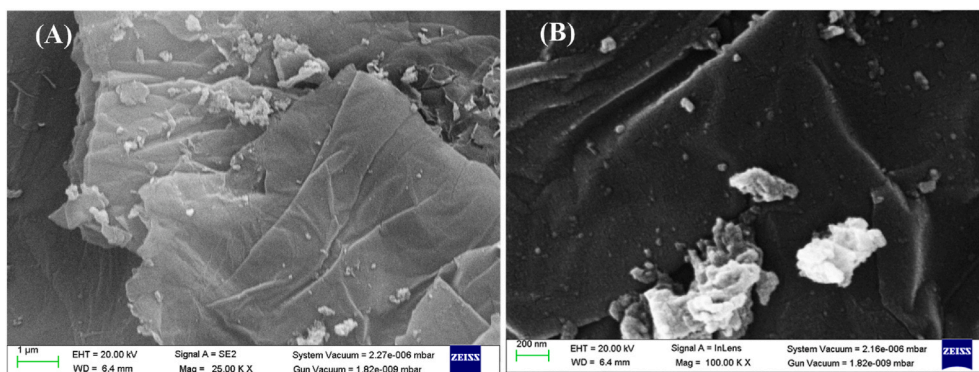**Fig. 3.** TGA graph of rGO-NiO nanocomposite.
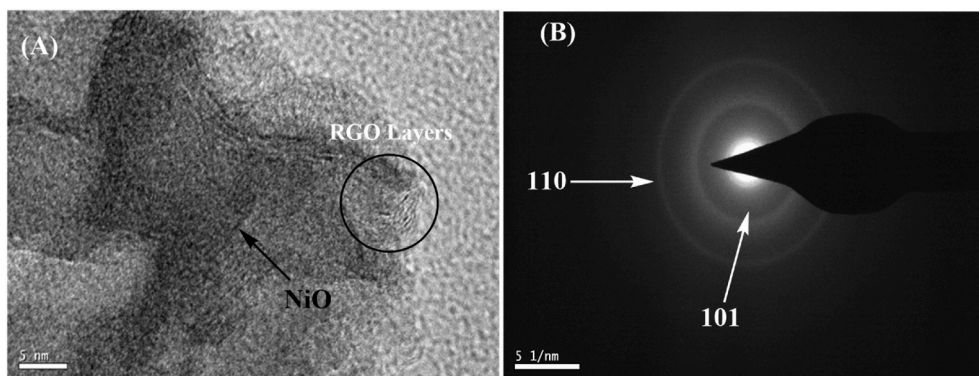

Fig. 4. (A, B) SEM images of rGO-NiO catalyst.

Fig. 5. (A) TEM images (B) SAED image for the prepared catalyst.

Table 2
Element table of rGO-NiO nanocomposite.

Element	Weight%	Atomic%
O	42.73	73.25
Ni	57.27	26.75

disorder in the materials (Fig. 6(a)). The initial GO has an ID/IG of 0.84. The Raman spectra of rGO-NiO shows the D (1352.4 cm^{-1}) and G (1585.4 cm^{-1}) bands of chemically reduced graphene oxide with an intensity ratio is 0.85, as well as peaks at 531 and 1062 cm^{-1} attribute to NiO shaking peaks [26] (Fig. 6(b)). The peaks at 536 cm^{-1} attributed to NiO's first order transverse optical and longitudinal optical phonon modes, respectively. The peak at 1073 cm^{-1} may be attributed to NiO's second order transverse and longitudinal optical phonon modes [26].

XPS spectra is also confirm the formation of prepared catalyst. XPS is performed (Figs. 7 and 8), to identify the number of element and to confirm the binding between NiO composites and GO. The Ni2p high-resolution XPS spectrum comprises four individual peaks at 853.3 eV, 861.2 eV, 870.6 eV, and 876.5 eV. The peaks at 853.3 eV and 861.2 eV allotted to Ni2p3/2 and its satellite, while the peaks at 870.6 eV and 876.5 eV due to Ni2p1/2 and its satellite.

3.1. Catalytic reduction

RGO-NiO catalyst is used for reduction of 4-NA and picric acid. Reduction of 4-NA and picric acid are examined by using UV spectroscopy (Fig. 9). After every 10 min, UV of reduction reaction of 4-NA was taken. From Fig. 9(a), it is very clear that, with increasing the time of reaction, % of reduction of the 4-NA is increases. Reduction of 4-nitro-aniline is 97% in 130 min as shown in Fig. 9 (a). Reduction of picric acid is 60% in 30 min as shown in Fig. 9 (b).

3.2. Removal of ARS dye by using different catalyst

Fig. 10 shows the UV spectra of Alizarin dye in aqueous media before and after 1 h of removal by using prepared catalyst with 100 ppm of dye. In initial reading, the peak of ARS at 420 nm. However, after removal, the peak of ARS shifted at 383 nm [27,28]. RGO-NiO shows the 47% removal after 1 h.

Fig. 11 shows the UV spectra of Indigo dye in aqueous media before and after 4 h of removal by using prepared catalyst with 100 ppm of dye. In initial reading, the peak of dye at 663 nm [29,30]. RGO-NiO shows the 62% removal of dye from aqueous media after 4 h.

3.3. Effect of dye concentration

To observe the effect of concentration of ARS dye on removal onto rGO-NiO nanocomposite is performed in a concentration rage of 100 ppm, 200 ppm, 300 ppm, 400 ppm, and 500 ppm (Fig. 12). The UV spectra indicate the increasing the dye concentration, removal of dye is also increases. 500 ppm of the solution shows highest dye removal (90%) in 90 min [31]. Table 3, shows the effect of dye concentration on Alizarin Red S dye.

To observe the effect of concentration of indigo dye on removal onto rGO-NiO nanocomposite is performed in a concentration range of 100 ppm, 200 ppm, 300 ppm, 400 ppm, and 500 ppm (Fig. 13). The UV spectra indicate the decreasing the removal of dye while increasing the dye concentration. 100 ppm solution of the dye shows highest dye removal (62%) in 4 h. Table 4 shows the effect of dye concentration on Indigo dye.

3.4. Re-useability of the catalyst

After the successful conversion of nitro compounds to amino products, the catalyst is separated completely from the reaction mixture by using filter paper and then washed with water followed by ethyl acetate to remove trace products present on the surface of the catalyst. And recovered catalyst is used up to five cycles (Table 5).

3.5. Kinetic study

The reduction of 4-NO$_2$ aniline is studied kinetically. As illustrated in Fig. 14, the process followed pseudo-first order kinetics since its R^2 value was 0.9122. The study of adsorption kinetics is critical for the analysis of adsorption rate and equilibrium time.

4. Conclusion

RGO-NiO is successfully prepared for reduction of picric acid, 4-nitro-aniline and removal of Alizarin Red S dye and Indigo dye from aqueous media. Prepared catalyst is characterized by using SEM with EDX, HR-TEM, XRD, TGA, XPS, Raman spectroscopy, and FTIR. In addition, reduction reaction and removal of dye are confirmed by UV–Vis spectroscopy.

Author contribution statement

Renu Verma: Performed the experiments; Wrote the paper.
Manmohan Singh Chauhan: Conceived and designed the experiments.
Saurabh Pandey: Analyzed and interpreted the data.
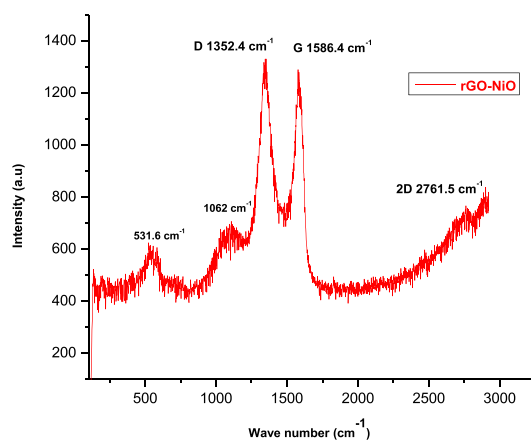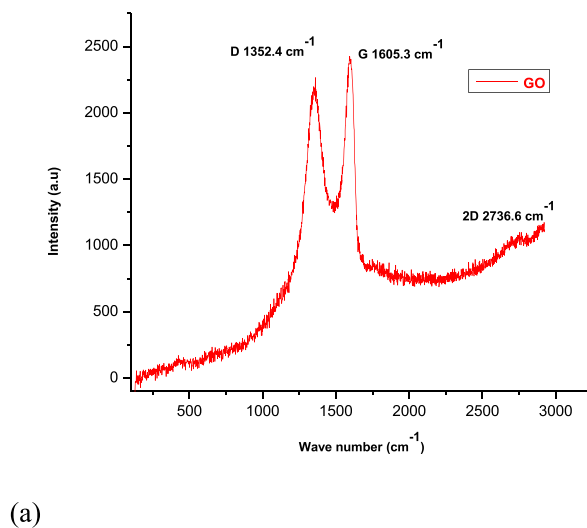Anshu Dandia: Contributed reagents, materials, analysis tools or data.

(a)

(b)

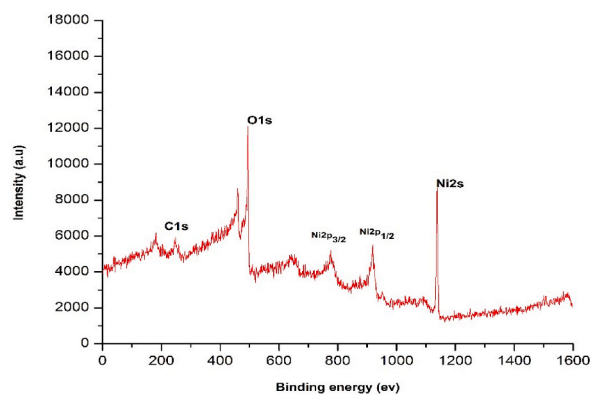**Fig. 6.** Raman Spectra of (a) GO and (b) rGO-NiO.
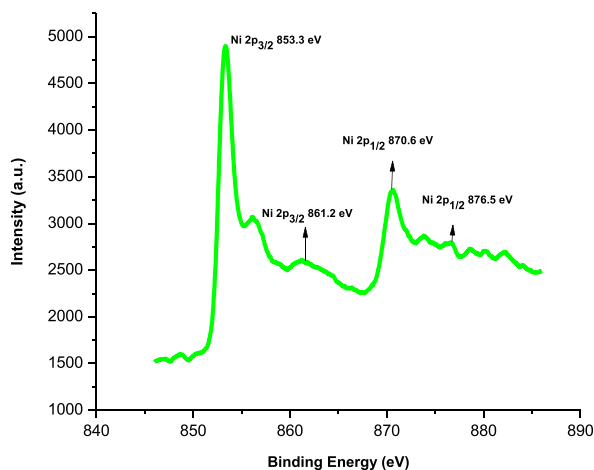

Fig. 7. XPS analysis survey of C1s, O1s, Ni.

Fig. 8. XPS graph for Ni 2p spectra of rGO-NiO nanocomposites.
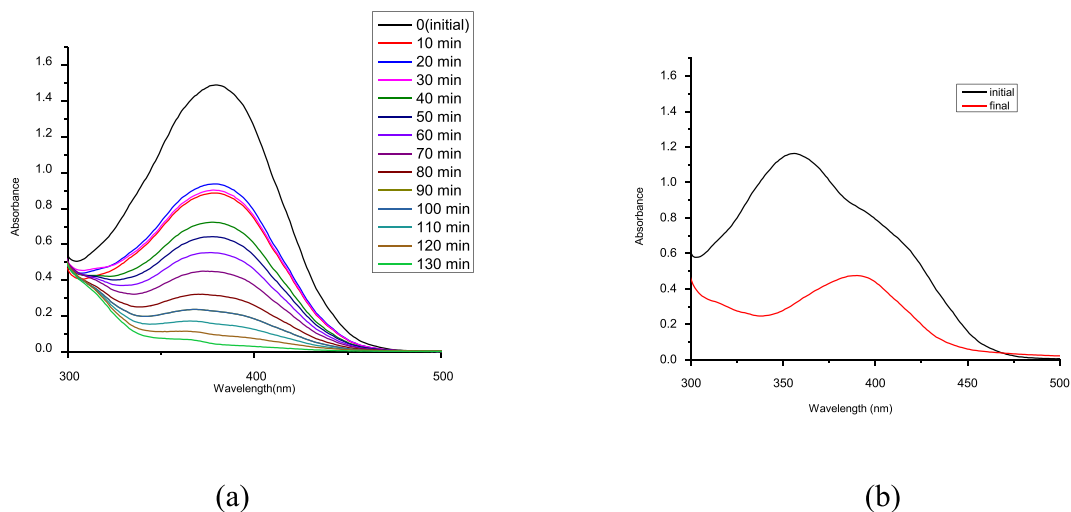

(a)   (b)

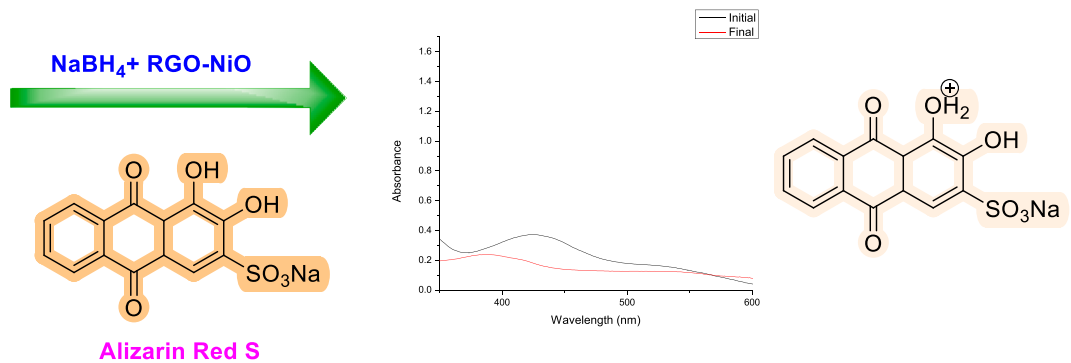**Fig. 9.** (a) UV–Vis plot of reduction of 4-NA, (b) UV–Vis plot of reduction of picric acid.

Fig. 10. Removal of ARS dye by using prepared catalyst.

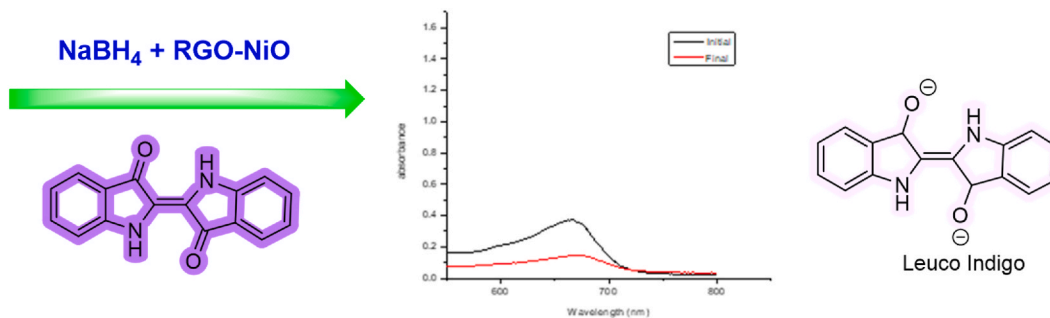**Fig. 11.** Removal of Indigo dye by using prepared catalyst.
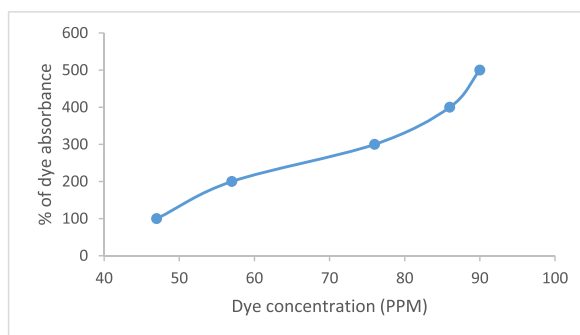

Fig. 12. Graph of removal of Alizarin Red S dye at different concentration of dye

Table 3
Effect of dye concentration on Alizarin Red S dye.

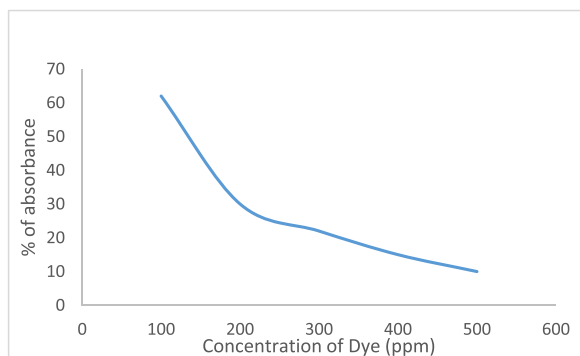| Entry	Dye Concentration (PPm)	% of dye degradation
1	100	47
2	200	57
3	300	76
4	400	86
5	500	89

Fig. 13. Plot of removal of Indigo dye at different concentration of dye.

Table 4
Effect of dye concentration on Indigo dye.

Entry	Dye Concentration (PPm)	% of dye degradation
1	100	62
2	200	30
3	300	22
4	400	15
5	500	10

Table 5
Re-useability of rGO-NiO nanocomposite.

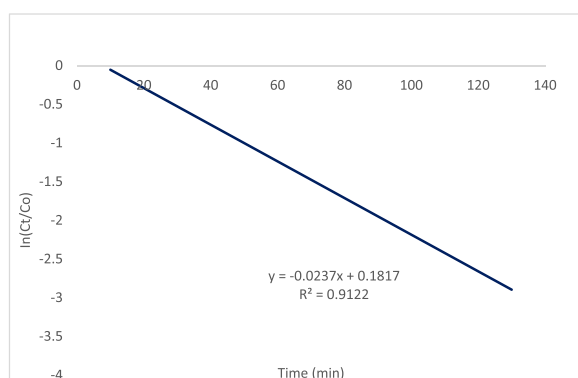| Number of cycles	% of conversion
1	97
2	97
3	92
4	92
5	90

Fig. 14. Kinetic study for reduction of 4-NO$_2$ aniline.

Data availability statement

Data included in article/supp. Material/referenced in article.

Funding

Declaration of competing interest

The authors declare that they have no known competing financial interests or personal relationships that could have appeared to influence the work reported in this paper.

Acknowledgement

References

[1] G.R. Delpiano, D. Tocco, L. Medda, E. Magner, A. Salis, Adsorption of malachite green and alizarin red s dyes using fe-btc metal organic framework as adsorbent, Int. J. Mol. Sci. 22 (2021) 1–16, https://doi.org/10.3390/ijms22020788.

[2] M.Y. Khan, M. Ahmad, S. Sadaf, S. Iqbal, F. Nawaz, J. Iqbal, Visible light active indigo dye/graphene/WO3 nanocomposites with excellent photocatalytic activity, J. Mater. Res. Technol. 8 (2019) 3261–3269, https://doi.org/10.1016/j.jmrt.2019.05.015.

[3] S. Jeon, J.W. Ko, W.B. Ko, Catalytic reduction of ortho - and meta -nitroaniline by nickel oxide nanoparticles, Natura (Milan) 55 (2020) 191–198.

[4] M.J. Iqbal, M.N. Ashiq, Adsorption of dyes from aqueous solutions on activated charcoal, J. Hazard Mater. 139 (2007) 57–66, https://doi.org/10.1016/j.jhazmat.2006.06.007.

[5] J. Terres, R. Battisti, J. Andreaus, P.C. De Jesus, Decolorization and degradation of Indigo Carmine dye from aqueous solution catalyzed by horseradish peroxidase, Biocatal. Biotransform. 32 (2014) 64–73, https://doi.org/10.3109/10242422.2013.873416.

[6] S. Hu, D. Yuan, Y. Liu, L. Zhao, H. Guo, Q. Niu, W. Zong, R. Liu, The toxic effects of alizarin red S on catalase at the molecular level, RSC Adv. 9 (2019) 33368–33377, https://doi.org/10.1039/c9ra02986a.

[7] L.D. Ardila-Leal, R.A. Poutou-Pinales, A.M. Pedroza-Rodriguez, B.E. Quevedo-Hidalgo, A brief history of colour, the environmental impact of synthetic dyes and removal by using laccases, Molecules 26 (2021), https://doi.org/10.3390/molecules26133813.

[8] K. Zhang, H. Li, X. Xu, H. Yu, Synthesis of reduced graphene oxide/NiO nanocomposites for the removal of Cr(VI) from aqueous water by adsorption, Microporous Mesoporous Mater. 255 (2018) 7–14, https://doi.org/10.1016/j.micromeso.2017.07.037.

[9] W. Wu, S. Liang, Y. Chen, L. Shen, H. Zheng, L. Wu, High efficient photocatalytic reduction of 4-nitroaniline to p-phenylenediamine over microcrystalline SrBi 2Nb 2O 9, Catal. Commun. 17 (2012) 39–42, https://doi.org/10.1016/j.catcom.2011.10.012.

[10] D. Chen, J. Ye, Hierarchical WO3 hollow shells: dendrite, sphere, dumbbell, and their photocatalytic properties, Adv. Funct. Mater. 18 (2008) 1922–1928, https://doi.org/10.1002/adfm.200701468.

[11] S. Chen, H. Zhang, X. Yu, W. Liu, Photocatalytic reduction of nitrobenzene by titanium dioxide powder, Chin. J. Chem. 28 (2010) 21–26, https://doi.org/10.1002/cjoc.201090030.

[12] G. Liu, X. Li, J. Zhao, S. Horikoshi, H. Hidaka, Photooxidation mechanism of dye alizarin red in TiO2 dispersions under visible illumination: an experimental and theoretical examination, J. Mol. Catal. Chem. 153 (2000) 221–229, https://doi.org/10.1016/S1381-1169(99)00351-9.

[13] J. Wang, Z. Yuan, R. Nie, Z. Hou, X. Zheng, Hydrogenation of nitrobenzene to aniline over silica gel supported nickel catalysts, Ind. Eng. Chem. Res. 49 (2010) 4664–4669, https://doi.org/10.1021/ie1002069.

[14] M. Kheirabadi, M. Samadi, E. Asadian, Y. Zhou, C. Dong, J. Zhang, A.Z. Moshfegh, Well-designed Ag/ZnO/3D graphene structure for dye removal: adsorption, photocatalysis and physical separation capabilities, J. Colloid Interface Sci. 537 (2019) 66–78, https://doi.org/10.1016/j.jcis.2018.10.102.

[15] M.H.H. Ali, A.D. Al-Afify, M.E. Goher, Preparation and characterization of graphene – TiO2 nanocomposite for enhanced photodegradation of Rhodamine-B dye, Egypt J Aquat Res 44 (2018) 263–270, https://doi.org/10.1016/j.ejar.2018.11.009.

[16] A.A. Al-Kahtani, Photocatalytic degradation of rhodamine B dye in wastewater using gelatin/CuS/PVA nanocomposites under solar light irradiation, J. Biomaterials Nanobiotechnol. 8 (2017) 66–82, https://doi.org/10.4236/jbnb.2017.81005.

[17] R. Giovannetti, E. Rommozzi, M. Zannotti, C.A. D'Amato, Recent advances in graphene based TiO2 nanocomposites (GTiO2Ns) for photocatalytic degradation of synthetic dyes, Catalysts 7 (2017), https://doi.org/10.3390/catal7100305.

[18] P.B. Arthi G, L. Bd, A simple approach to stepwise synthesis of graphene oxide nanomaterial, J. Nanomed. Nanotechnol. 6 (2015) 1–4, https://doi.org/10.4172/2157-7439.1000253.

[19] S. Korkmaz, A. Kariper, Graphene and graphene oxide based aerogels: synthesis, characteristics and supercapacitor applications, J. Energy Storage 27 (2020), https://doi.org/10.1016/j.est.2019.101038.

[20] L. Sun, H. Yu, B. Fugetsu, Graphene oxide adsorption enhanced by in situ reduction with sodium hydrosulfite to remove acridine orange from aqueous solution, J. Hazard Mater. 203–204 (2012) 101–110, https://doi.org/10.1016/j.jhazmat.2011.11.097.

[21] A. Al-Nafiey, A. Kumar, M. Kumar, A. Addad, B. Sieber, S. Szunerits, R. Boukherroub, S.L. Jain, Nickel oxide nanoparticles grafted on reduced graphene oxide (rGO/NiO) as efficient photocatalyst for reduction of nitroaromatics under visible light irradiation, J. Photochem. Photobiol. Chem. 336 (2017) 198–207, https://doi.org/10.1016/j.jphotochem.2016.12.023.

[22] S. Thenmozhi, T. Krishnaveni, K. Kadirvelu, Reduction of nitrocompounds in aqueous medium using electrospun MgO nanofibers, Mater. Res. Express 6 (2019), https://doi.org/10.1088/2053-1591/ab0b05.

[23] F. Wang, D. Zhao, L. Zhang, L. Fan, X. Zhang, S. Hu, Nanostructured nickel nitride with reduced graphene oxide composite bifunctional electrocatalysts for an efficient water-urea splitting, Nanomaterials 9 (2019) 1–7, https://doi.org/10.3390/nano9111583.

[24] A. Roychoudhury, A. Prateek, S. Basu, S.K. Jha, Preparation and characterization of reduced graphene oxide supported nickel oxide nanoparticle-based platform for sensor applications, J. Nanoparticle Res. 20 (2018), https://doi.org/10.1007/s11051-018-4173-y.

[25] K. Bhowmik, A. Mukherjee, M.K. Mishra, G. De, Stable Ni Nanoparticle–Reduced graphene oxide composites for.pdf, Langmuir 30 (2014) 3209–3216.

[26] N. Mironova-Ulmane, A. Kuzmin, I. Steins, J. Grabis, I. Sildos, M. Pars, Raman scattering in nanosized nickel oxide NiO, J Phys Conf Ser 93 (2007), https://doi.org/10.1088/1742-6596/93/1/012039.

[27] K. Saeed, N. Zada, I. Khan, Photocatalytic degradation of alizarin red dye in aqueous medium using carbon nanotubes/Cu–Ti oxide composites, Separ. Sci. Technol. 54 (2019) 2729–2737, https://doi.org/10.1080/01496395.2018.1552296.

[28] P. Zucca, C.M.B. Neves, M.M.Q. Simoes, M.S. Neves, G. Cocco, E. Sanjust, Immobilized lignin peroxidase-like metalloporphyrins as reusable catalysts in oxidative bleaching of industrial dyes, Molecules 21 (2016), https://doi.org/10.3390/molecules21070964.

[29] J. Wang, L. Lu, F. Feng, Improving the indigo carmine decolorization ability of a bacillus amyloliquefaciens laccase by site-directed mutagenesis, Catalysts 7 (2017), https://doi.org/10.3390/catal7090275.

[30] B.Y. Buyukakinci, N. Sokmen, Investigation of indigo dyeing using sodium borohydride as reducing agent, CBU Int. Conference Proceedings. 5 (2017) 1061–1063, https://doi.org/10.12955/cbup.v5.1071.

[31] U. Jinendra, D. Bilehal, B.M. Nagabhushana, A.P. Kumar, Adsorptive removal of Rhodamine B dye from aqueous solution by using graphene–based nickel nanocomposite, Heliyon 7 (2021), e06851, https://doi.org/10.1016/j.heliyon.2021.e06851.